Journal of Nuclear Materials 573 (2023) 154124

Contents lists available at ScienceDirect

Journal of Nuclear Materials

journal homepage: www.elsevier.com/locate/jnucmat

The bonding of H in Zr under strain

J. Smutna[a], M.R. Wenman[a], A.P. Horsfield[a,*], P.A. Burr[b]

[a] Imperial College London, Department of Materials, South Kensington Campus, London, SW7 2AZ, UK
[b] University of New South Wales, School of Mechanical and Manufacturing Engineering, Sydney, NSW 2052, Australia

ARTICLE INFO

Article history:
Received 5 September 2022
Revised 27 October 2022
Accepted 3 November 2022
Available online 4 November 2022

Keywords:
Zirconium
Hydrogen
Dislocation
Embedded atom method
Density functional theory

ABSTRACT

Accurate computer simulation is important for understanding the role of irradiation-induced defects in zirconium alloys found in nuclear reactors. Of particular interest is the distribution and trapping of hydrogen, and the formation of zirconium hydride. These simulations require an accurate representation of Zr-H bonding in order to predict the behaviour of H around atomic-scale defects, dislocation lines, and dislocation loops. Here we explore the bonding of H in Zr under strain, how well it is represented by state-of-the-art Embedded Atom Method (EAM) potentials, and what physics is needed for an accurate representation in a Linear Combination of Atomic Orbitals (LCAO) Density Functional Theory (DFT) framework. For H in dilute solution under hydrostatic strain in the range -10% to +10%, solution energies and Zr-H bond lengths computed using EAM potentials are found to be in poor agreement with plane-wave DFT results. We note that the bond lengths are in a poor agreement even in equilibrium. LCAO basis sets are used to explore the importance of electron distribution around H atoms, and the transfer of electrons between H and Zr. The electron distribution around H atoms is found to be important to the explanation of the difference between octahedral and tetrahedral interstitial sites for H, with H in a tetrahedral site having very similar bonding to H in zirconium hydrides. The interatomic electron transfer has a smaller impact but is needed for maximum accuracy.

1. Introduction

The interaction of hydrogen with zirconium is of a great interest in the nuclear industry. When H atoms penetrate into the metal matrix, they diffuse according to the stress gradients. The H diffusion is further complicated by the presence of defects, some of which can trap a significant number of H atoms (9 for a vacancy at 0K) [1]. Once the local H concentration exceeds the solubility limit, zirconium hydrides precipitate, eventually leading to embrittlement of the material and possibly to delayed hydride cracking [2]. While these phenomena have been studied by a range of experimental techniques, the distribution of H can be hard to quantify, especially on the scale of dislocation loops or smaller defects, which are very common in irradiated material.

Zirconium-hydrogen interactions have also been a subject for computational modelling. At the continuum scale, the interaction of H with strained Zr can be described by linear elasticity theory by using the elastic dipole tensor of H, the solubility of H, and other parameters from atomistic simulations or experiment [3]. Other continuum techniques, such as phase field modelling, also require a large number of parameters. While in theory these models could also include defects (such as dislocations and dislocation loops), this would again require more input from smaller scale simulations or numerical optimisation.

Small dislocation loops and dislocation lines can be simulated directly at the atomic scale. While very small dislocation loops are just on the edge of our current computational ability for density functional theory (DFT) [4], empirical potentials can readily be used for these simulations. In fact, a number of previous papers use empirical potentials to look at diffusion of hydrogen near dislocation loops, attempting to quantify the amount of H near the loops at a given temperature using molecular dynamics [5,6]. While the potentials are typically fit to DFT calculations, for interactions between hydrogen and point defects in Zr, the correct behaviour in the strained environment around a dislocation loop has not been tested.

The strain fields around dislocations determine the long range interaction with other dislocations and point defects, and thus are important for the dynamics of the system of which they are a part. They are thus also discussed in this work. While they are not purely hydrostatic, we believe that the poor performance of the two empirical potentials for hydrostatic strain could transfer

* Corresponding author.
E-mail address: a.horsfield@imperial.ac.uk (A.P. Horsfield).

https://doi.org/10.1016/j.jnucmat.2022.154124

to more complicated strain fields. However, given that hydrostatic strain changes volume, while shear does not, making the connection is not completely straightforward. The performance in shear and uniaxial strains deserves more exploration.

There are a range of computational techniques available to us to study the behaviour of H in Zr. We employ three of them in this work: Embedded Atom Potentials (EAM), Density Functional Theory (DFT) with a plane wave (PW) basis, and DFT with a Linear Combination of Atomic Orbitals (LCAO) basis set. As already hinted at above, they each have advantages and disadvantages: by using all three we aim to increase the amount of reliable information about the systems we can obtain. In brief, EAM enables the largest scale simulations to be performed at reasonable cost, and thus allows the effect of varying system parameters (such as cell size and strain) to be explored efficiently. However, its accuracy is not always sufficient. Plane wave DFT enables accurate reference values to be computed with some confidence, and thus provides useful reference data. LCAO DFT can be faster than PW DFT, but also can be less accurate. However, it retains enough accuracy to provide useful insight, and the formalism lends itself naturally to interpretation of results in terms of atomic and bond properties.

In this work we evaluate the performance of two of the current state-of-the-art Embedded Atom Method (EAM) potentials for the Zr-H system under hydrostatic strain: one is the Zr-H potential developed by Maxwell et al. [7], which is based on the widely used MA#3 potential for pure Zr [8]; the other is the BMD19.2 potential [5]. These potentials have been specifically selected because of their suitability for modelling of H in solution, and most notably their ability to predict the correct ground state interstitial site for H. While H is found to be more stable in the tetrahedral site by both *ab initio* calculations [1] and experimentally [9], other empirical potentials available in the literature predict the larger octahedral site to be more stable than the tetrahedral site. We note that main focus of this work is not to criticise existing potentials, but to explore why they fail and therefore what changes or additions are needed to represent this bonding accurately.

Electronic structure methods are able to provide an accurate description of bonding. However, with traditional plane-wave DFT it can be difficult to analyse the local bonding because of the non-local nature of the basis set. An LCAO technique has been used which allows for a simple attribution of electronic density to atoms, as well as allowing further approximations. This helps us to identify the physical phenomena that are important for the interactions, helping us to build simpler models. The main phenomenon investigated is charge transfer, both between different atoms, and between different atomic orbitals on one atom. While the primary focus is on H in dilute solution, the differences between the interactions involving H in solution and in hydrides is also discussed. This work builds on our previous work on pure Zr [10], allowing this paper to focus on the representation of hydrogen. Most importantly, a large part of this work has been dedicated to the choice of an appropriate basis set and its implications for the processes important to bonding.

We note that zero-point motion of hydrogen was not included in our calculations. It has been found to change the values of interstitial formation energies [11], though not the energy ordering of the octahedral and tetrahedral sites. Given the greatly increased computational cost associated with computing phonon spectra we have just computed total energies of the structures.

2. Methods

As noted above, several different methods for atomic scale simulation are used in this work, and their results are compared. All simulations use atomic relaxation at 0 K, with a fixed supercell size. Plane-wave DFT calculations were performed as a reference. To describe the electron-nucleus interactions, for Zr we used ultrasoft pseudopotentials to represent the 1s, 2s, 2p, 3s, 3p and 3d electrons implicitly, while electrons in the 4s, 4p, 4d, 5s and 5p orbitals were modelled explicitly. For H, we used an on-the-fly (OTF) pseudopotential generated by CASTEP to represent the nucleus. These calculations were performed with the CASTEP software [12], using a plane-wave energy cutoff of 450 eV [13] and the exchange and correlation functional of Perdew, Burke, and Ernzerhof (PBE) [14]. We used a $20 \times 20 \times 12$ grid of k points to sample the Brillouin zone for the hcp unit cell of Zr and derived the grid for larger cells from that [13].

Calculations with empirical EAM potentials were performed using the LAMMPS code [15], with an interface provided by the Atomistic Simulation Environment (ASE) Python package [16]. Two recent EAM potentials were studied in order to find out their suitability for simulations of interstitial H in elastically strained Zr, namely the BMD19.2 potential [5] and the MA#3 potential [8] with the terms for H developed by Maxwell et al. [7]. While many other empirical potentials are available in the literature [17–19], none of them is able to reproduce the ordering of the solution energy of H in different interstitial sites at zero pressure: instead they predict the ground state site for H to be in the larger octahedral site, in disagreement with both DFT results and experiments [9,20].

All other simulations for intermediate models were performed using the PLATO code [21,22]. The main advantages of PLATO are: the ability to use a range of approximations with the same basis set; the availability of tools for straightforward building of different atom-centered basis sets for use with LCAO DFT and tight binding models. This allows us to get a better understanding of the physics involved in H-Zr interactions, and what ingredients are needed to represent it accurately.

The theory behind the LCAO method, and the approximations used to go from LCAO to tight binding, are described in detail in our previous work [10]. Here, we only highlight the most relevant parts of the theory. Two levels of theory have been used in this paper: the full Kohn-Sham functional, which includes electronic self-consistency, and the Harris-Foulkes functional, which approximates the former by not including self-consistency. For the Harris-Foulkes functional we start from the superposition of atomic electron densities, and only one iteration is performed to find an approximate total energy and electron density. Unfortunately, the current implementation in PLATO only enables single-point energy calculations, so for the Harris functional calculations only, the structures relaxed using plane-wave DFT have been used to evaluate the performance. The possibility of using 2-centre tight binding for this system is also briefly discussed.

The main questions for the LCAO model are: what are the optimal choices of pseudopotential and basis set? As this work is a continuation of the development of tight binding models for Zr, we have decided to keep the same GTH-LDA-q4 pseudopotential [23] and *4d 5p* basis set with a radial cutoff of 7.3 a_0 (Bohr radii), as in the previous work [10]. This has shown reasonable results for bulk Zr for all LCAO calculations considered, and allowed better computational efficiency than more complex or more extended basis sets. For H, the GTH-PBE-q1 pseudopotential was used [24], and a range of basis sets were considered. The suitability of basis set choice also provides some insight into the physics of H in Zr. Both the basis set confinement radius r_0 and the orbitals included were varied. The orbitals used were based on atomic orbitals of an atom in a confinement potential given by

$$V(r) = \left(\frac{r}{r_0}\right)^6 \tag{1}$$

where r_0 is a confinement radius and r is the distance from the centre of the atom, and the orbitals go to zero at $r_{cut} = r_0 + 1.0\,a_0$. When appropriate, the orbitals were split into a long-range and

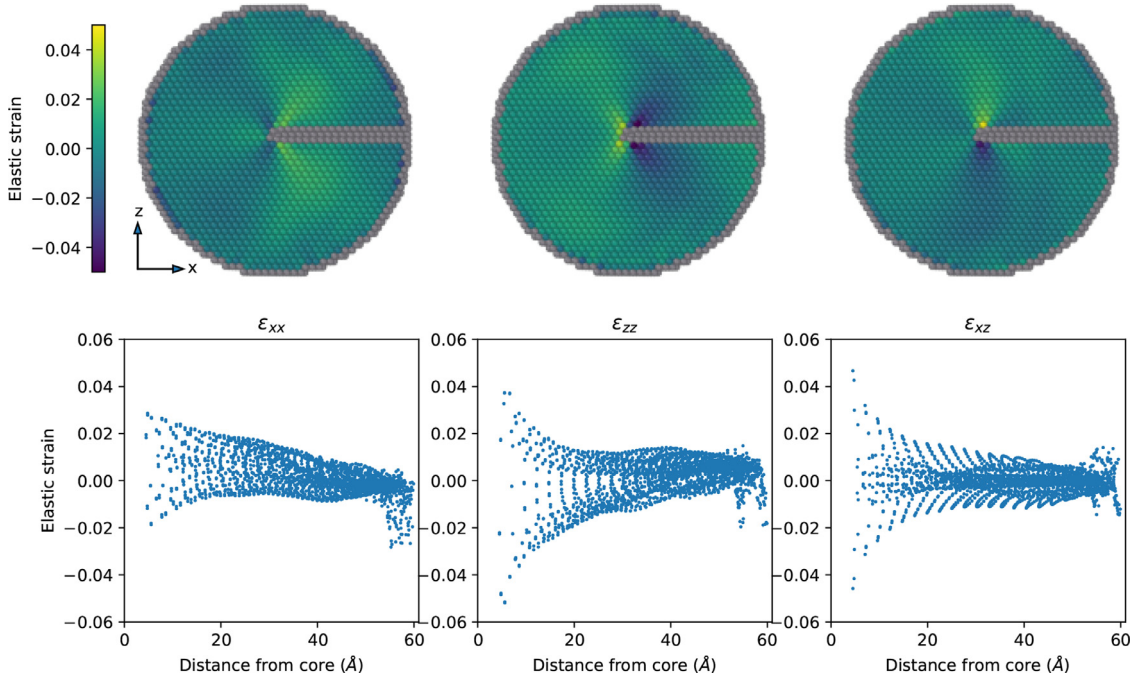

Fig. 1. The elastic strains for the structure identified as HCP by OVITO for a $\langle c/2 \rangle_{ext}$ edge dislocation, as a function of distance from the core. The atoms identified as other structures are shown in grey and not included in the scatter plots — these belong to the dislocation core, the stacking fault and the edge of the simulation where atoms are in contact with vacuum. The configuration was obtained using the MA EAM#3 potential [8].

a short-range part following the same formalism as SIESTA [25]. When these split (double-ζ) orbitals are used, the long-range part is marked by a star in the remainder of this paper.

The focus of this paper is on hydrogen interstitial sites in zirconium, therefore the majority of calculations were performed for this system. A supercell of $3 \times 3 \times 2$ hcp unit cells, with a single H atom in either an octahedral or a tetrahedral interstitial site has been used. We performed a systematic convergence test with cells sizes ranging from 37 atoms to 289 atoms, and found the H solution energy changes by much less than 0.01 eV. A k-point grid of $10 \times 10 \times 10$ was used for all DFT calculations (plane-wave and LCAO). A hydrostatic strain has been applied over the range -10% to + 10%, keeping the c/a ratio to 1.6 for all simulations. Note that negative pressures correspond to negative strains (compressive), and positive pressures correspond to positive strains (tensile). While using such a small supercell could lead to errors in the solution energies calculated due to the elastic interactions between the periodic images, the energy difference between H being in the octahedral and tetrahedral interstitial sites is only slightly affected (about 5 meV) [26]. Similarly, fixing the c/a ratio does affect the results (pure Zr under compression has a c/a ratio closer to ideal [27]), however the variation of c/a ratio with pressure is not necessarily the same for all models considered, and constant pressure calculations were not implemented in PLATO. While the latter issue could have been easily remedied, it was better to reduce the number of variables that affect the final results. Other systems, namely zirconium hydrides (ZrH and ZrH_2) were also briefly considered, with unit cells containing 4 Zr atoms and 4 and 8 H atoms in tetrahedral sites respectively. The k-point grid used here was $7 \times 7 \times 8$.

3. Results

This section focuses on two key aspects of the predictions for interstitial H, which are directly comparable in all models considered. First, the solution energy is considered, calculated as

$$E_{sol} = E_{Zr_{36}H} - E_{Zr_{36}} - 1/2E_{H_2}, \tag{2}$$

where $E_{Zr_{36}H}$, $E_{Zr_{36}}$ and E_{H_2} are total energies of the pure Zr supercell, the same supercell with interstitial H, and a hydrogen dimer respectively. This calculation is problematic for empirical potentials because the two EAM potentials are not fitted to give reasonable results for a H dimer in vacuum, and therefore predict an incorrect energy or bond length for this dimer. Therefore, we have set $E_{H_2} = -3.029$ eV and $E_{H_2} = -4.718$ eV for Maxwell *et al.* and BMD19.2 potentials respectively, leading to an agreement of solution energies with plane-wave DFT results at zero strain. While this introduces a shift to the solution energy, this shift is the same for all calculated solution energies for a given empirical potential.

Second, the atomic structure was also compared. This comparison was achieved by calculating the bond lengths between H and its nearest neighbour Zr atoms. In the case of an octahedral site, all 6 of the nearest neighbours are symmetry equivalent. For the tetrahedral site, there are three equivalent bonds between H and Zr atoms which are all in the same basal plane, and one bond in the direction of the c-axis.

3.1. Strains around the dislocation core

To determine the strains around the dislocation core we created a cylinder of Zr with the dislocation running through it along the direction of the axis. Periodic boundaries were applied along the direction of the axis, with free boundaries applied in the other directions. We used the MA#3 potential to describe the interaction between the Zr atoms.

The environments of several types of straight dislocation lines were analysed using the OVITO software and principal and deviatoric strains of up to about 5% were found near the dislocation line (this only includes the atoms identified as belonging to an HCP structure, not atoms in the core). The results for a $\langle c \rangle$ type dislocation with an extrinsic stacking fault are shown in Fig. 1, and are representative of strains around both $\langle c \rangle$ and $\langle a \rangle$ type disloca-

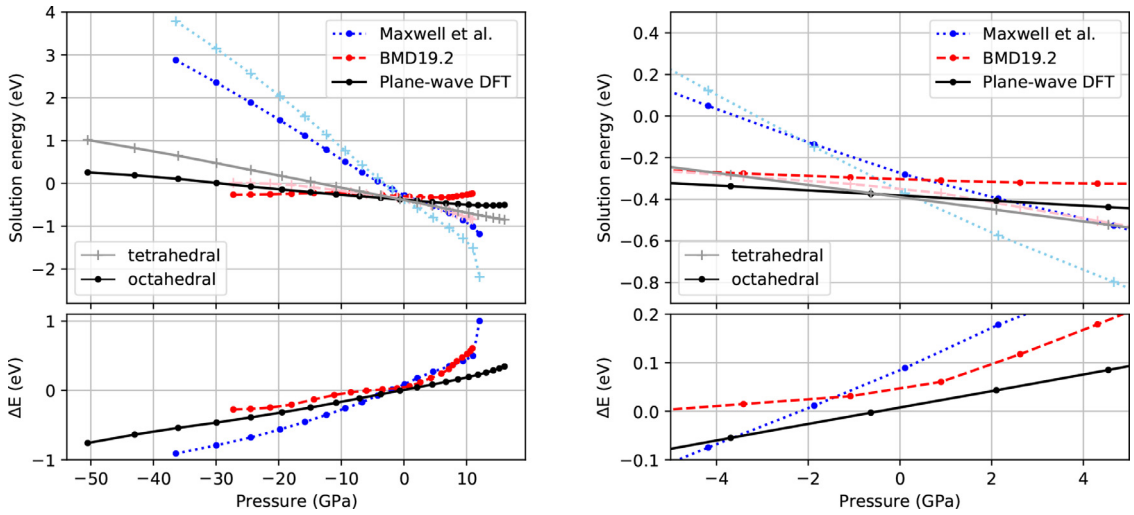

Fig. 2. Solution energy for H under hydrostatic pressure calculated using EAM potentials, with plane-wave DFT results included as a reference. For all methods, the lattice constants were strained between 90 and 110% of their equilibrium value, except for the Maxwell et al. potential, for which calculations with strain above 107% did not converge. More detail around low pressures is shown on the right. The symbol ΔE corresponds to the difference in solution energy between H in the octahedral site and in the tetrahedral site.

tions; significant hydrostatic strains were not present around screw dislocations. Results from Fig. 1 are in agreement with the strains around dislocation loops in Fe [28]. While the hydrostatic strains applied in this work are not directly representative of the deformation around loops, notably with no shear or uni-axial strain being modelled, it is unlikely that a model would perform better for these more complicated strain environments than for the hydrostatic strain case alone.

3.2. Performance of empirical potentials

The empirical potentials considered here were specifically selected because at zero pressure, they predict the tetrahedral site to be lower in energy than the octahedral one, with a difference of 0.092 eV for Maxwell et al. [7] and 0.039 eV for the BMD19.2 potential [5], compared to 0.061 eV from plane-wave DFT [1]. Note that the DFT value varies slightly between different sources, but is always between 0.04 eV and 0.08 eV [1,29–31]. Because of the smaller supercell used here, the difference in solution energies calculated vary slightly, and were 0.084, 0.040 and 0.053 eV using the Maxwell et al. potential, BMD19.2 potential and plane-wave DFT (this work) respectively. The error is much smaller than the energy changes with strain, so the small supercell will have a negligible effect.

As shown by Fig. 2, applying tensile hydrostatic strain to the supercell leads to a lowering of the solution energy, with H in the octahedral site being more sensitive to this strain. Under compressive stress larger than ∼1 GPa the octahedral site becomes more energetically favourable. However, the rate of change of the solution energy with pressure varies considerably between the different methods. The slope is much steeper for the Maxwell et al. potential than the reference DFT results. The BMD19.2 potential has a more similar slope to DFT, but varies depending on the pressure and even becomes positive for an octahedral site in tension. The range of pressures for which the empirical potentials produce reliable results is also limited; however the pressures explored here, corresponding to the lattice constant varying from 90% to 110% of their equilibrium values, are rather extreme even on a local, atomistic scale. We also note that the near linear variation of energy with strain seen for the plane-wave DFT results suggests linear elasticity might be an appropriate method to estimate the interaction energy between the H interstitials and the strain field.

Comparing the Zr-H bond lengths computed using different methods (Fig. 3) exposes the shortcomings of these potentials to represent H in solution under hydrostatic strain. The octahedral site is represented reasonably well by both potentials, but the bonds are shorter (for both potentials) and the gradient changes more steeply with pressure (for the BMD19.2 potential) compared to DFT. Additionally, the tetrahedral site geometry is poorly described by both potentials. The potential developed by Maxwell et al. predicts *c*-axis bonds to be shorter than the basal ones, in disagreement with DFT. For the BMD19.2 potential, the bond length variation would suggest that at high compressive pressures, the bond length actually increases: this might actually be the H atom attempting to migrate to a different site, but this behaviour is not observed in DFT calculations. Even at near equilibrium pressures, the bond lengths of the tetrahedral hydrogen are smaller, more different from each other and vary more with pressure than the DFT results. Therefore, even though the energy differences between the two interstitial sites at equilibrium matches DFT quite well, the geometries do not.

The empirical potentials are therefore not very good at representing H in Zr under hydrostatic strain, and become less reliable further from equilibrium. This is likely to affect the behaviour that these potentials predict for H in the strain field of dislocation loops. In particular, the drive to areas of tensile strain is too large for both empirical potentials.

3.3. Basis set selection

Just as for the zirconium model discussed in our previous work [10], when finding a suitable basis set, a sensible starting point is starting with a small basis set, in this case only containing a *1s* orbital. We then generate basis sets with varying cutoff radii and compare how they predict properties for these structures. Two approaches have been explored in this work, differing in the structures they used. Since they are complementary, we present them both here.

3.3.1. Hydride densities of states

While we are mainly interested in H in solution in HCP Zr in this paper, the work presented here originated in an effort to design a model capable of representing both H in solution and zirconium hydrides. Therefore, it made sense to use a stochiometric hy-

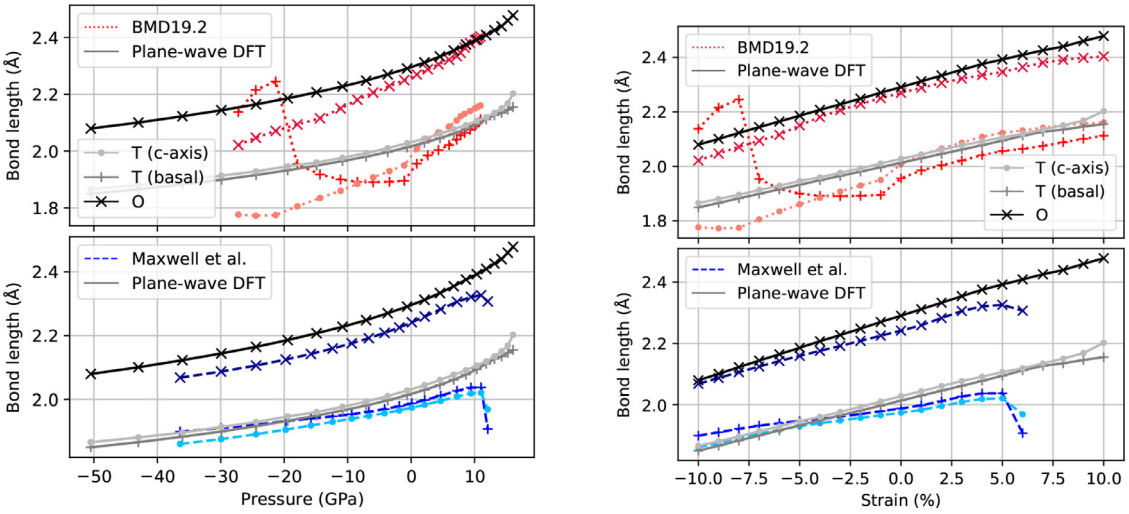

Fig. 3. The length of Zr-H nearest neighbour bonds for H under hydrostatic pressure calculated using EAM potentials, with plane-wave results included as a reference. For more details, see Fig. 2.

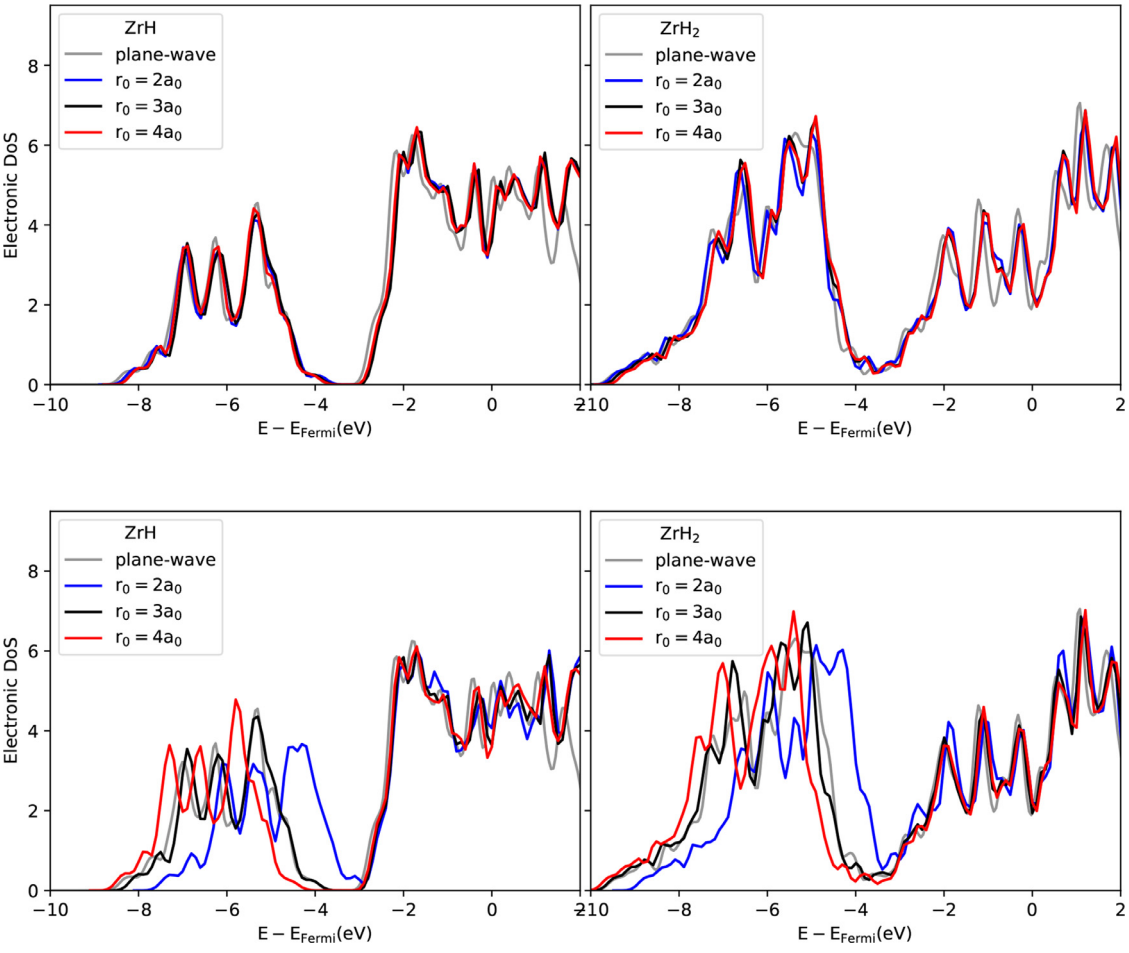

Fig. 4. Electronic density of state for ZrH (left) and ZrH_2 (right), predicted using a *1s* basis set with different confinement radii with the Kohn-Sham functional (top) and the Harris-Foulkes functional (bottom).

dride as a reference structure (ZrH in the ϵ structure in this case), and compare the equilibrium volume and density of states with a DFT calculation.

When comparing the densities of states of Fig. 4 for different basis sets, the main change is in the position of the states below the band gap located 3 eV below the Fermi energy when the Harris-Foulkes functional is used. These states shift to higher energies for shorter-ranged basis sets, and lower energies for longer-ranged ones. When a Kohn-Sham functional is used, the confinement radius hardly affects the density of states - self-consistency adds some robustness to the model and makes it less reliant on the choice of r_0. The best agreement with plane-wave DFT (the lowest

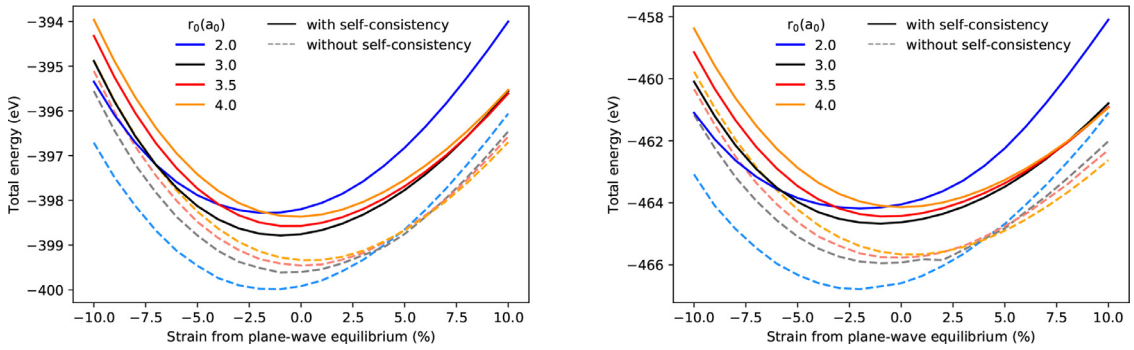

Fig. 5. Total energy variation with hydrostatic strain from equilibrium (as predicted by plane-wave calculations) for ZrH (left) and ZrH_2 (right), predicted using a *1s* basis set with different confinement radii and with and without self-consistency.

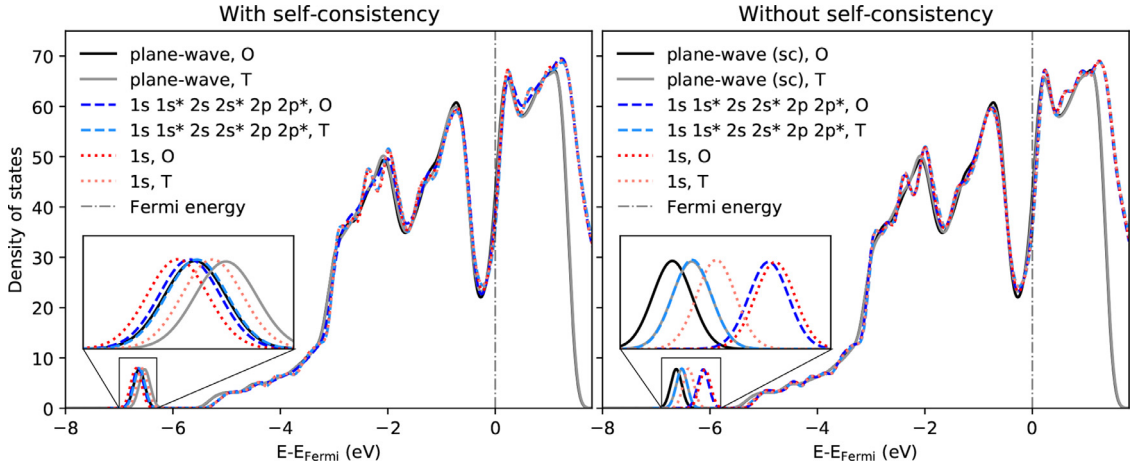

Fig. 6. Electronic density of state for interstitial H atom in octahedral (O) or tetrahedral (T) site, predicted using different basis sets, all using r_0=3.0 a_0 and different levels of theory.

energy near equilibrium) is found with the confinement radius of $r_0 = 3.0a_0$. This basis set also predicts an equilibrium volume close to the DFT value (Fig. 5) both with and without self-consistency.

The sensitivity of the self-consistent calculations to r_0 proves that the consideration of both structural and electronic properties is important, and only the former is sensitive to the choice of r_0 when self-consistency is included (at least in the case of ZrH). The error in the energy is second-order in the error in electron density, while the density of states is first order. Hence using a better approximation to the real electron density (resulting from the Kohn-Sham functional) instead of only a first order correction to atomic densities (Harris-Foulkes functional) affects the density of states more than the minimum energy configurations. Reassuringly, for $r_0 = 3.0a_0$, the densities of states with and without self-consistency are in good agreement, further supporting the choice of this confinement radius.

In the next step, it is important to consider the transferability of this basis set to other structures. Here, we take another stochiometric hydride, ZrH_2 in the γ structure, and the hcp-Zr structures with an interstitial H atom. As can be seen in Figs. 4 and 5, the agreement of the densities of states and equilibrium volume is very good for ZrH_2. However, the results do not look as good for the interstitial H (Fig. 6), where the H peaks in the density of states do not compare well to the plane-wave DFT results (mainly in the case without self-consistency), and the predicted solution energies have the wrong ordering Fig. 7. This suggests that H in solution is quite different from hydrides: for example, the electron cloud could be more or less spread out from the core, or even not well represented by a spherical basis set. In any case, the structures with interstitial H need to be used to choose a basis set that represents them well.

3.3.2. Total energy of interstitial H

The variation of total energy for H in the tetrahedral and octahedral sites using the *1s* basis set is shown in Fig. 7. For the *1s* basis set, the tetrahedral H atom seems to be better represented by a slightly shorter ranged basis set. Interestingly, the basis set we previously picked for hydrides, i.e. a *1s* orbital with $r_0 = 3.0a_0$, has a confinement radius in between $2.5a_0$, which gives the lowest total energy for H in the tetrahedral site, and $3.75a_0$ for the octahedral site. More concerning, even for these two "ideal" basis sets, i.e. $r_0 = 2.5a_0$ for the tetrahedral H and $r_0 = 3.75a_0$ for the octahedral one, the total energy of the H in the octahedral site is lower than in the tetrahedral site, in disagreement with plane-wave DFT. The basis set functions could have the wrong shape, but this is less easy to explore systematically, so an easier solution is to use a larger basis set.

3.3.3. Expanding the basis set

To start, we have used a relatively large basis set (*1s 1s* 2s 2s* 2p 2p**) to determine the best confinement radius. Just like in the previous section, we have plotted the total energy as a function of the confinement distance (Fig. 7). All the total energies calculated for this basis set are significantly lower than for the *1s* basis set, meaning that expanding the basis set does indeed lead to finding a state closer to the true ground state. For all radii considered, the

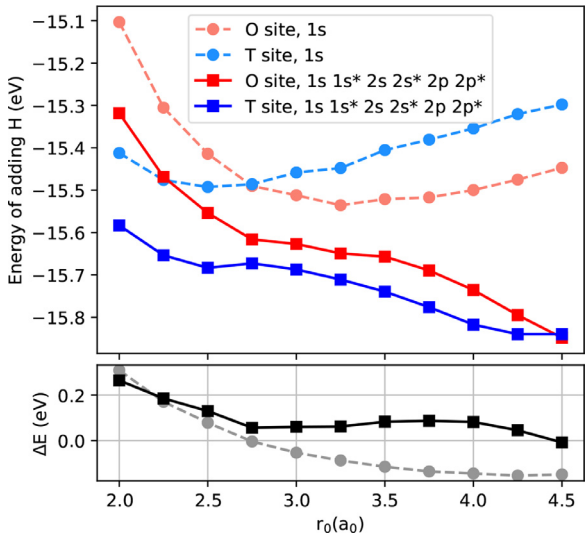

Fig. 7. The energy of adding H into a Zr cell is the difference in energy between the cell with Zr plus an H atom, and the cell with just Zr. In this figure the variation of this energy with the confinement potential radius for the H basis sets, for H in tetrahedral and octahedral sites, is presented. This directly corresponds to the total energy with a shift equal to the total energy of the bulk Zr supercell. The energy difference is defined as $\Delta E = E_{oct} - E_{tet}$.

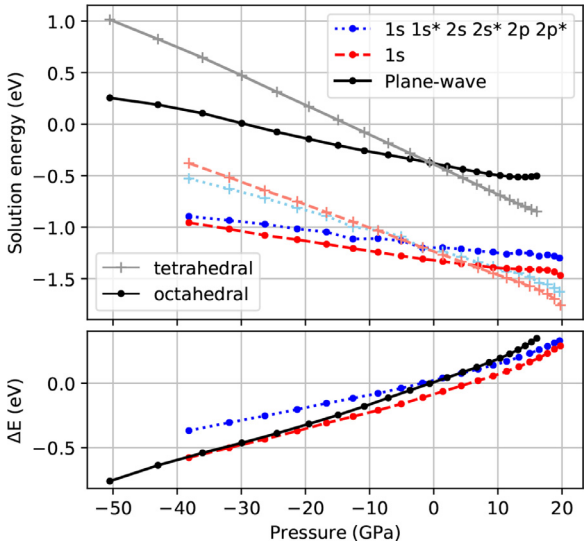

Fig. 8. Solution energy for H under hydrostatic pressure calculated using Kohn-Sham LCAO DFT, with plane-wave results included as a reference. The energy difference is defined as $\Delta E = E_{oct} - E_{tet}$.

total energy of the configurations with tetrahedral H is lower than ones with octahedral H, with the difference being ~0.06 eV for all $2.75a_0 \leq r_0 \leq 3.0a_0$. However, for both structures the total energy keeps decreasing with increasing basis set range. While this could be due to a better representation of the electron density around H, it could also be caused by providing additional states for electron density around Zr. For the rest of this work, we have chosen the $r_0 = 4.0a_0$, as the predicted difference in energy is reasonable, the short range improves computational efficiency and it also agrees with confinement of the *1s* only basis set considered in the previous section.

The density of states predicted by the *1s 1s* 2s 2s* 2p 2p** basis set is much closer to plane-wave DFT predictions than using only a *1s* basis set (Fig. 6). The variation of solution energy and Zr-H bond lengths with pressure agree quite well with plane-wave DFT results for both basis sets (Fig. 8). In fact, while the *1s* basis set predicts the octahedral site to be lower in energy at 0 GPa, the ordering changes at 4 GPa (in tension). This does suggest that even the small *1s* basis is relatively good, but the energy difference between the two sites is so small a more extensive basis set is needed. For both basis sets we also see that the calculated solution energy is significantly lower than desired. This could be for several reasons, the most likely one being that this basis set, despite being quite flexible, optimised for H in Zr is not very good at representing a H dimer, predicting a higher total energy for it and therefore leading to low solution energy. Secondly, the Zr-H bond lengths predicted from the LCAO basis sets are all slightly too short compared to plane-wave DFT (Fig. 9). This is actually caused by the pure Zr model, which predicts a slightly too small equilibrium volume for an hcp Zr cell, meaning that the pressure calculated for the same size bulk Zr supercell with plane-wave and LCAO DFT predicts higher pressure for the latter. In fact, when plotted against the strain, the agreement with plane-wave and our extended basis set is be much better.

For the *1s 1s* 2s 2s* 2p 2p** basis set Mulliken population analysis reveals very little filling of the *2p* orbitals; the next step is therefore to try to reduce the basis set size. Using a confinement radius $r_0 = 3.0a_0$, we have generated a range of basis sets with different orbitals included, some of them split, and evaluated the predicted solution energy difference between the two sites: these are listed in Table 1. Unsurprisingly, the total energies for the intermediate basis sets are in between the values for the two limiting basis sets. While splitting the *1s* orbitals into a double-ζ is not sufficient, adding a *2s* or a *2p* orbital results in the tetrahedral site being more stable, with the addition of a *2s* orbital resulting in a larger difference between the two sites. However, the smallest basis set predicting an energy difference comparable to that from plane-wave DFT calculations contains *1s 1s* 2s 2s** orbitals. Therefore, while adding the flexibility to the radial part of the basis set is important for this problem, the angular dependency is not needed.

The remaining question is why this radial flexibility is needed. Is the local electron density very different between H in the tetrahedral and octahedral sites, or are both of them quite similar, but very different from the "squeezed free atom" simplification at the root of building our basis set? In order to answer this, we have partitioned the energy density to obtain the density around each atom.

The partition function for site i is defined as

$$w_i(\vec{r}) = \frac{\rho_i^{(0)}(|\vec{r} - \vec{R}_i|)}{\sum_j \rho_j^{(0)}(|\vec{r} - \vec{R}_j|)} \tag{3}$$

with $\rho_i^{(0)}$ being the atomic electron density distribution for the confined atom i (i.e. an atom with one filled state corresponding to the *1s* orbital for H), and $\vec{R}_i$ is the position of atom i. The partitioned atomic density for atom i is then:

$$\rho_i(\vec{r}) = w_i(\vec{r})\rho(\vec{r}). \tag{4}$$

where $\rho(\vec{r})$ is the electron density of the entire system. Note that $\sum_i w_i(\vec{r}) = 1$ so that $\sum_i \rho_i(\vec{r}) = \rho(\vec{r})$.

The atomic density assigned to each atom can then be further decomposed into its spherical harmonic components:

$$\rho_{ilm}(r) = \int \rho_i(\vec{r}) Y_{lm}^*(\hat{r}) d\hat{r} \tag{5}$$

where Y_{lm} are spherical harmonics and the integral is performed over the unit circle centred on atom i for a range of radii up to the cutoff of $\rho_i(r)$. Note that this atomic electron density as defined here can have components corresponding to higher l values than the angular momentum quantum numbers of the basis set compo-

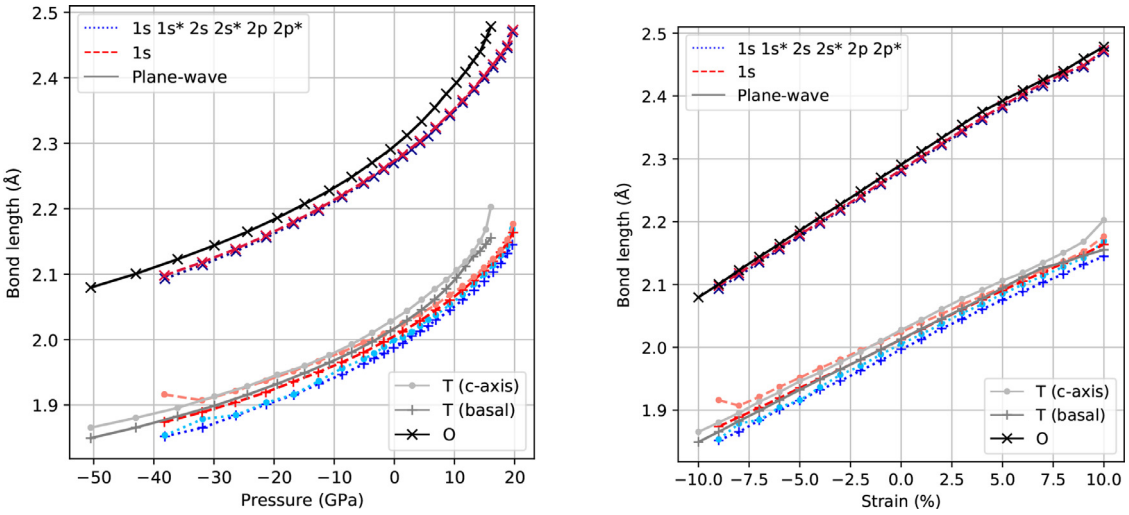

Fig. 9. Zr-H nearest neighbour bond length for H in octaherdal or tetrahedral interstitial sites under hydrostatic pressure calculated using Kohn-Sham LCAO DFT, with plane-wave results included as a reference.

Table 1
The change in solution energy based on the orbitals included in the hydrogen basis set in unstrained structures. Negative difference in solution energy indicates that octahedral site is more stable than tetrahedral one.

Basis set	Tetrahedral H total energy (eV)	Octahedral H total energy (eV)	Difference in total energies (eV)
1s	-3009.51	-3009.57	-0.054
*1s 1s**	-3009.59	-3009.59	0.000
1s 1s 2p*	-3009.65	-3009.64	0.002
1s 1s 2p 2p**	-3009.67	-3009.66	0.013
1s 1s 2s*	-3009.63	-3009.61	0.020
1s 1s 2s 2p*	-3009.68	-3009.66	0.021
1s 2s	-3009.61	-3009.58	0.030
1s 1s 2s 2s**	-3009.66	-3009.61	0.045
1s 1s 2s 2s* 2p*	-3009.71	-3009.66	0.045
1s 1s 2s 2s* 2p 2p**	-3009.74	-3009.68	0.060

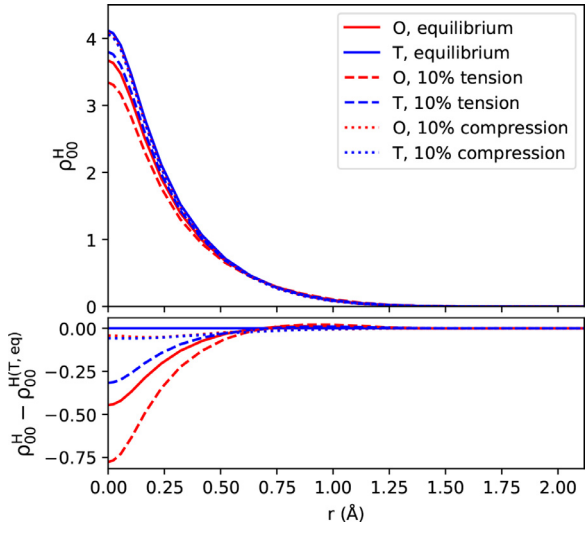

Fig. 10. Spherically symmetric part of the partitioned electron density belonging to H atom in interstitial sites. The bottom plot shows the difference between the electron densities compared to a reference of tetrahedral site at equilibrium.

nents, but should nevertheless provide a good comparison tool for the electron density around H atoms in different sites.

Figures 10 and 11 show the comparison of the projected electron density for $l = 0$ and $l = 1, m = 0, 1, 2$ for H in the two sites, as well as the difference between the two. The angular variation, captured by the latter term, is larger for the tetrahedral site than the octahedral site, as expected from the shape of the site, however it is essentially negligible for both sites. The radial part appears quite similar, though the electron density of the tetrahedral site is larger in the centre, while the octahedral site has more density further from the centre. Similar trends can be seen for these structures under strain. They are both much more different from the squeezed *1s* orbital than from each other.

3.4. Further approximations

One of the original aims of this work was to create a faster model, capable of modelling a larger number of atoms than traditional plane-wave DFT. We have already shown that the LCAO approximation performs relatively well, and while the PLATO implementation is oriented more towards detailed analysis than computational efficiency, it could be used in software such as CP2K, which are more computationally efficient. PLATO also allows us to explore the possibility of further approximations in the physics. These further simplifications have a potential to significantly shorten the computational time, but they must not remove any essential physics from the Zr-H model.

We focus on two areas of simplification: the removal of electronic self-consistency and the removal of many-centre interactions. The importance of these should be useful for the creation of better empirical surrogate models.

3.4.1. Harris-Foulkes functional

In order to remove self-consistency we have used the Harris-Foulkes functional instead of the Kohn-Sham functional, and again calculated the solution energies and densities of states for the zero

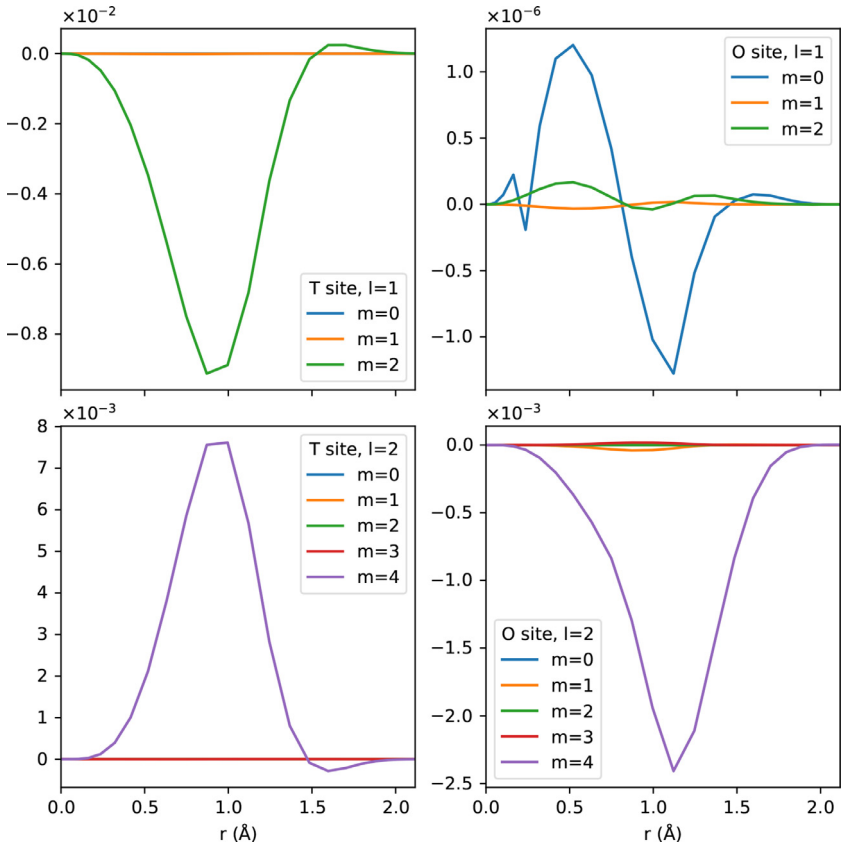

Fig. 11. Non-spherically symmetric parts of the partitioned electron density belonging to H atom in interstitial sites.

pressure case. Since atomic relaxation was not currently implemented in the software, we have used atomic configurations calculated from plane-wave calculations. Without self-consistency and using the *1s* basis set, H in the tetrahedral has a higher solution energy than in the octahedral site, by 0.106 eV. For the *1s 1s* 2s 2s* 2p 2p** basis set, the solution energy ordering is correct, but the difference of 0.032 eV is slightly less than the self-consistent value. In both cases, the density of states is a much worse fit to the plane-wave density, with the two H peaks being further apart and ordered differently than in plane-wave calculations (Fig. 6). Therefore, electronic transfer is important for the H-Zr interaction. This agrees with the intuitive picture expected from comparing electronegativity of H (2.1) and Zr (1.3), predicting the H to be somewhat negatively charged. The sensitivity to the choice of basis set provides good evidence that the on-site electronic transfer between different orbitals is very important, as the density is very different from a free or confined atom and varies with strain. For zirconium hydrides, the story is similar to H in solution in HCP Zr. Structural properties such as the equilibrium volume are in good agreement with self-consistent results (Fig. 5), while the electronic density is more affected and more dependent on the chosen confinement radius (Fig. 4).

3.4.2. 2-Centre approximation

In previous work [10], we have already shown that there are problems with the 2-centre approximation when looking at self-interstitial atoms. Due to the current efforts of several research groups around the world to create 2-centre tight binding models for metals which include interstitial elements such as H, we have explored the importance of many-centre effects (and therefore the suitability of 2-centre tight binding) for modelling of H in Zr, and we believe that the results will be qualitatively similar for other metals.

The inverse Slater-Koster method described in our earlier work [10] has been used to find effective 2-centre hopping integrals calculated from a many-centre LCAO DFT Hamiltonian matrix. This projection was done independently for pairs of atoms. For H in solution, Fig. 12 shows a significantly larger magnitude of hopping integrals for some Zr-Zr bonds: these correspond to bonds between Zr atoms neighbouring the H atom (highlighted in grey) and to bonds going directly through the H in an octahedral site (highlighted in pink). So, even the presence of a small H atom adds significant many-centre contributions to all hopping integrals of the surrounding metal. This effect is the largest for the orbitals that extend furthest from the core.

This many-centre effect is even more significant when we consider the hydrides. Here, the real many-centre nature of the hopping integrals becomes apparent for H-H bonds too. As can be seen in Fig. 13, while 2 H atoms in next-nearest neighbour positions have almost negligible hopping integrals when there is no atom directly in between them, the presence of the Zr atom half way between them makes their interaction comparable to the nearest neighbour ones. This analysis only includes *1s-1s* σ hopping integrals, which are closest to the core, and would be bigger for more extended orbitals. Two centre tight binding models are therefore even less suitable to model hydrides than they are for H in dilute solution, even if we only want to model hydrides.

4. Discussion

The first takeaway from the results presented is that neither of the current state-of-the-art EAM potentials provides a sufficiently accurate description of the behaviour of H in strained bulk Zr to

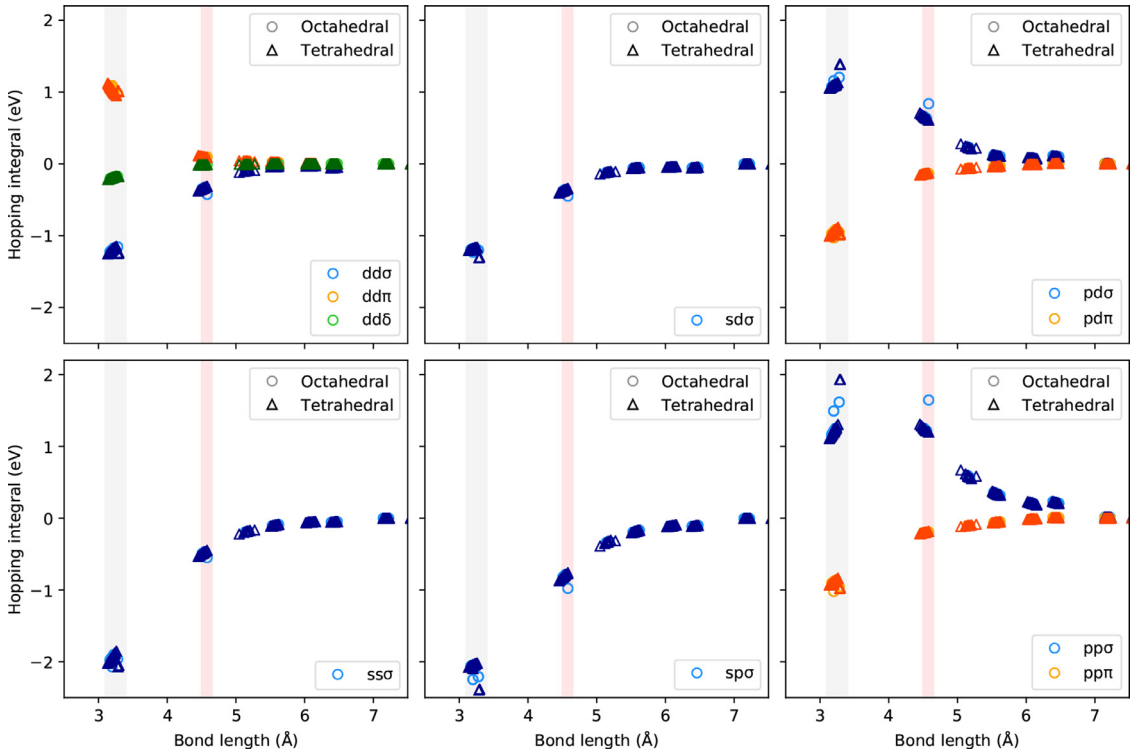

Fig. 12. The projected 2-centre hopping integrals for Zr-Zr bonds in equilibrium HCP structures with an interstitial H atom. The shaded areas correspond to the bond lengths for Zr atoms directly neighbouring the H atom (gray) and bonds going directly through the H atom (pink, in the case of H in the octahedral site).

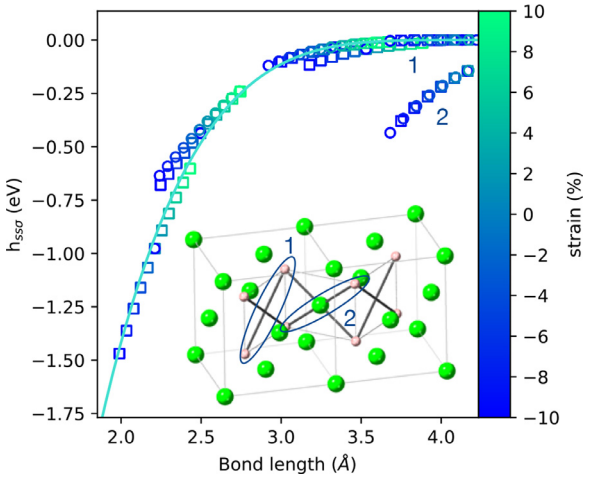

Fig. 13. The H-H $ss\sigma$ hopping integrals in zirconium hydrides. The two-centre hopping integral from a dimer (solid line) compared the effective ones for the ZrH (circles) and ZrH_2 (squares) for a range of uniform strains. The inset shows a ZrH crystal, with the two types of bond of length in the range 3.5 to 4.3 Å highlighted; the ones without a Zr atom in the middle (1) are well approximated by the dimer while the ones with it (2) are significantly different.

model the distribution of hydrogen in the environment of dislocations, where large atomistic strains and gradients are present. In particular, the variation of the solution energy with respect to pressure is not in full quantitative agreement with *ab initio* calculations, meaning that diffusion in environments with a gradient in strain field would likely not be well represented. For instance, the energy gained from moving from a non-deformed area (unstrained) to an area with 5% hydrostatic strain (representative of a crystal in proximity to a dislocation) is 0.32 eV from the DFT calculations, compared to 1.13 eV from Maxwell et al. The BMD19.2 potential agrees with the DFT calculation, predicting 0.31 eV, however shows much poorer agreement for the octahedal site, which is part of the diffusion pathway for H in Zr, and in areas of compression where H would be depleted. One of the aims of developing EAM potentials is their ability to model large systems, such as the environment of a dislocation loop, and run molecular dynamics simulations for these systems as presented, for instance, in the paper introducing the BMD19 potential [5]. As the environment of a dislocation loop is strained, with both shear and normal strains present, the accuracy of the results needs further investigation.

In this work, the strains considered were more than double those we found in the dislocation environment, so the failure of the EAM potentials in high pressure conditions shown is unlikely to be as important as it would initially appear. When deciding on the suitability of a potential for studying H in Zr, especially if it is intended to be used for modelling dislocation loops, we believe that the solution energy of H in strained lattices should be an important factor to consider when performing the fitting. This is paramount when modelling hydrogen diffusion in deformed environments. Related to the strain energy associated with H in Zr is the elastic dipole tensor. This is relevant to the diffusion of H in an elastic field and should also be included.

The observations made about the bonding of H in Zr should be helpful for the creation of simplified models in general, not just EAM. We have shown the importance of electronic self-consistency, and transfer of electronic charge to H atoms. Since a different amount of charge is transferred depending on the site the H atom is in, it should probably be modelled explicitly. The charge transfer from Zr to H is likely to be a reason behind the ground state of H being in the tetrahedral interstitial site despite this site being smaller than the octahedral site. We find that H in a tetrahedral site attracts more charge, probably due to the closeness of the Zr atoms: the larger the charge is, the more it is concentrated near the core of the H atom.

The charge transfer also varies with strain, with the H charge increasing with increasing compressive strain. While in the cases

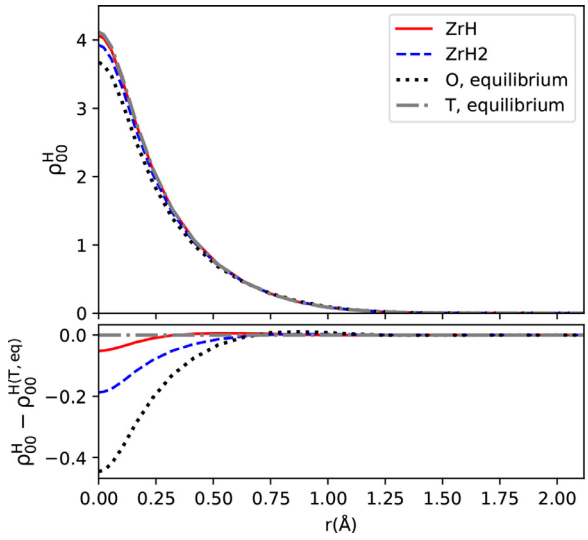

Fig. 14. Spherically symmetric part of the partitioned electron density belonging to H in zirconium hydrides compared to H in interstitial sites in HCP Zr.

we considered here the charge remains relatively spherical, this would likely change for shear strains or H in a vacancy, as the environment becomes less symmetric. However, the shear strains are unlikely to have a large influence on the solution energy as H is generally only considered to be attracted to areas of hydrostatic tension.

Despite hydrides initially appearing to have a different structure to an interstitial H in Zr, the bonding between H and Zr is actually very similar to H in a tetrahedral site in a HPC structure, as can be seen in Fig. 14. In fact, H sits in tetrahedral sites in an FCT structure in hydrides, so the similarity is not entirely surprising. The H atoms in the hydride are also largely screened from each other, and even for ZrH_2, the charge around the dilute H atoms is only slightly smaller than H in a tetrahedtal site in HCP Zr.

It should also be noted that while there is always a charge transfer to H from the surrounding Zr atoms, this is at most 0.2 *e*. While the definition of a charge is very sensitive to the choice of basis set and functional, and quantifying the charge transfer from DFT can be problematic, the relative values should still be comparable. When we started this work, we assumed that H was in an H^- state, and the peak in the density of states of H in solution corresponds to two states. However, while there are indeed two states available in the peak, they are split between the H atom and the neighbouring Zr atoms.

5. Conclusion

This work examined the bonding of H under hydrostatic strain range of ±10% and has found that current state-of-the-art EAM potentials are not yet able to represent these interactions sufficiently accurately for simulations of hydrogen in strained environments, such as those found around dislocations, despite providing an accurate description in unstrained Zr. We attribute this to the lack of explicit charge transfer in these models, and thus the lowering of the H interstitial formation energy in a tetrahedral site must be achieved by adjusting other parameters, which might create non-physical results.

By using different atom-centered basis sets for H in DFT calculations, we have found that to accurately represent H in different interstitial sites as well as in hydrides, a basis set with sufficient radial flexibility is needed. The shape of the electron density is quite different to that for a free H atom, which is more long-ranged. However, at least for the hydrostatic strains considered here, any non-radial components of the electron density are negligible.

Declaration of Competing Interest

The authors declare that they have no known competing financial interests or personal relationships that could have appeared to influence the work reported in this paper.

CRediT authorship contribution statement

J. Smutna: Investigation, Writing – original draft. **M.R. Wenman:** Funding acquisition, Conceptualization, Writing – review & editing, Supervision. **A.P. Horsfield:** Methodology, Writing – review & editing, Supervision. **P.A. Burr:** Validation, Writing – review & editing.

Acknowledgments

We acknowledge the preliminary work of Amelia Paine and Max Boleininger on the Zr tight binding model, which motivated this work. This work was supported through a studentship in the Centre for Doctoral Training on Theory and Simulation of Materials at Imperial College London funded by the EPSRC (EP/L015579/1) and Rolls-Royce. We acknowledge the Thomas Young Centre under grant number TYC-101. The computational resources were provided by the Research Computing Service at Imperial College London.

This work has in part been performed within the framework of the international MUZIC (Mechanistic Understanding of Zirconium Corrosion) program. The authors gratefully acknowledge the industrial support from EDF, EPRI, Naval Nuclear Laboratory, Rolls-Royce, Westinghouse and Jacobs.

References

[1] C. Domain, R. Besson, A. Legris, Atomic-scale Ab-initio study of the Zr-H system: I. Bulk properties, Acta Mater. 50 (13) (2002) 3513–3526, doi:10.1016/S1359-6454(02)00173-8.

[2] A.T. Motta, L. Capolungo, L.-Q. Chen, M.N. Cinbiz, M.R. Daymond, D.A. Koss, E. Lacroix, G. Pastore, P.-C.A. Simon, M.R. Tonks, B.D. Wirth, M.A. Zikry, Hydrogen in zirconium alloys: a review, J. Nucl. Mater. 518 (2019) 440–460, doi:10.1016/j.jnucmat.2019.02.042.

[3] M. Patel, L. Reali, A.P. Sutton, D.S. Balint, M.R. Wenman, A fast efficient multi-scale approach to modelling the development of hydride microstructures in zirconium alloys, Comput. Mater. Sci 190 (2021) 110279, doi:10.1016/j.commatsci.2021.110279.

[4] B. Christiaen, C. Domain, L. Thuinet, A. Ambard, A. Legris, A new scenario for <c> vacancy loop formation in zirconium based on atomic-scale modeling, Acta Mater. 179 (2019) 93–106, doi:10.1016/j.actamat.2019.07.030.

[5] E. Wimmer, M. Christensen, W. Wolf, W.H. Howland, B. Kammenzind, R.W. Smith, Hydrogen in zirconium: atomistic simulations of diffusion and interaction with defects using a new embedded atom method potential, J. Nucl. Mater. 532 (2020) 152055, doi:10.1016/j.jnucmat.2020.152055.

[6] M. Christensen, W. Wolf, C. Freeman, E. Wimmer, R.B. Adamson, L. Hallstadius, P.E. Cantonwine, E.V. Mader, Diffusion of point defects, nucleation of dislocation loops, and effect of hydrogen in hcp-Zr: Ab initio and classical simulations, J. Nucl. Mater. 460 (2015) 82–96, doi:10.1016/j.jnucmat.2015.02.013.

[7] C.I. Maxwell, E. Torres, J. Pencer, Molecular dynamics study of hydrogen-vacancy interactions in α-zirconium, J. Nucl. Mater. 511 (2018) 341–352, doi:10.1016/j.jnucmat.2018.09.012. Special Section on '18th International Conference on Fusion Reactor Materials'

[8] M.I. Mendelev, G.J. Ackland, Development of an interatomic potential for the simulation of phase transformations in zirconium, Philos. Mag. Lett. 87 (5) (2007) 349–359, doi:10.1080/09500830701191393.

[9] R. Khoda-Bakhsh, D. Ross, Determination of the hydrogen site occupation in the α phase of zirconium hydride and in the α and β phases of titanium hydride by inelastic neutron scattering, J. Phys. F Met. Phys. 12 (1982) 15–24.

[10] J. Smutna, R.M. Fogarty, M.R. Wenman, A.P. Horsfield, Systematic development of ab initio tight-binding models for hexagonal metals, Phys. Rev. Mater. 4 (2020) 043801, doi:10.1103/PhysRevMaterials.4.043801.

[11] M. Christensen, W. Wolf, C. Freeman, E. Wimmer, R.B. Adamson, L. Hallstadius, P.E. Cantonwine, E.V. Mader, H in α-Zr and in zirconium hydrides: solubility, effect on dimensional changes, and the role of defects, J. Phys. Condens. Matter 27 (2) (2014) 025402.

[12] S.J. Clark, M.D. Segall, C.J. Pickard, P.J. Hasnip, M.J. Probert, K. Refson, M.C. Payne, First principles methods using CASTEP, Z. Kristall. 220 (2005) 567–570.

[13] P. Burr, Ab-initio modelling of Zr and Be alloys for nuclear applications, Imperial College London, 2015 Ph.D. thesis.
[14] J.P. Perdew, K. Burke, M. Ernzerhof, Generalized gradient approximation made simple, Phys. Rev. Lett. 77 (18) (1996) 3865.
[15] S. Plimpton, Fast parallel algorithms for short-range molecular dynamics, J. Comput. Phys. 117 (1) (1995) 1–19, doi:10.1006/jcph.1995.1039.
[16] A.H. Larsen, J.J. Mortensen, J. Blomqvist, I.E. Castelli, R. Christensen, M. Dułak, J. Friis, M.N. Groves, B. Hammer, C. Hargus, E.D. Hermes, P.C. Jennings, P.B. Jensen, J. Kermode, J.R. Kitchin, E.L. Kolsbjerg, J. Kubal, K. Kaasbjerg, S. Lysgaard, J.B. Maronsson, T. Maxson, T. Olsen, L. Pastewka, A. Peterson, C. Rostgaard, J. Schiøtz, O. Schütt, M. Strange, K.S. Thygesen, T. Vegge, L. Vilhelmsen, M. Walter, Z. Zeng, K.W. Jacobsen, The atomic simulation environment—a python library for working with atoms, J. Phys. Condens. Matter 29 (27) (2017) 273002, doi:10.1088/1361-648x/aa680e.
[17] M.J. Noordhoek, T. Liang, Z. Lu, T.-R. Shan, S.B. Sinnott, S.R. Phillpot, Charge-optimized many-body (COMB) potential for zirconium, J. Nucl. Mater. 441 (1) (2013) 274–279, doi:10.1016/j.jnucmat.2013.06.004.
[18] M. Christensen, W. Wolf, C.M. Freeman, E. Wimmer, R.B. Adamson, L. Hallstadius, P.E. Cantonwine, E.V. Mader, Effect of alloying elements on the properties of Zr and the Zr–H system, J. Nucl. Mater. 445 (1) (2014) 241–250, doi:10.1016/j.jnucmat.2013.10.040.
[19] P. Chakraborty, A. Moitra, T. Saha-Dasgupta, Effect of hydrogen on degradation mechanism of zirconium: a molecular dynamics study, J. Nucl. Mater. 466 (2015) 172–178, doi:10.1016/j.jnucmat.2015.07.031.
[20] P.P. Narang, G.L. Paul, K.N.R. Taylor, Location of hydrogen in α-zirconium, J. Less Common Metals 56 (1) (1977) 125–128, doi:10.1016/0022-5088(77)90225-9.
[21] A.P. Horsfield, Efficient ab initio tight binding, Phys. Rev. B 56 (1997) 6594–6602, doi:10.1103/PhysRevB.56.6594.
[22] S.D. Kenny, A.P. Horsfield, Plato: a localised orbital based density functional theory code, Comput. Phys. Commun. 180 (2009) 2616–2621, doi:10.1016/j.cpc.2009.08.006.
[23] S. Goedecker, M. Teter, J. Hutter, Separable dual-space Gaussian pseudopotentials, Phys. Rev. B 54 (1996) 1703–1710, doi:10.1103/PhysRevB.54.1703.
[24] M. Krack, Pseudopotentials for H to Kr optimized for gradient-corrected exchange-correlation functionals, Theor. Chem. Acc. 114 (1) (2005) 145–152.
[25] J.M. Soler, E. Artacho, J.D. Gale, A. García, J. Junquera, P. Ordejón, D. Sánchez–Portal, The SIESTA method for ab initio order-n materials simulation, J. Phys. Condens. Matter 14 (11) (2002) 2745.
[26] P.A. Burr, S.T. Murphy, S.C. Lumley, M.R. Wenman, R.W. Grimes, Hydrogen solubility in zirconium intermetallic second phase particles, J. Nucl. Mater. 443 (1) (2013) 502–506, doi:10.1016/j.jnucmat.2013.07.060.
[27] H. Weekes, Synchrotron X-ray diffraction investigations into the micromechanics of hydrides in zircaloy-4, Imperial College London, 2015 Ph.D. thesis.
[28] T.M. Whiting, Modelling of solutes in ferritic reactor pressure vessel steels, Imperial College London, 2020 Ph.D. thesis.
[29] S.C. Lumley, R.W. Grimes, S.T. Murphy, P.A. Burr, A. Chroneos, P.R. Chard-Tuckey, M.R. Wenman, The thermodynamics of hydride precipitation: the importance of entropy, enthalpy and disorder, Acta Mater. 79 (2014) 351–362, doi:10.1016/j.actamat.2014.07.019.
[30] Y. Udagawa, M. Yamaguchi, H. Abe, N. Sekimura, T. Fuketa, Ab initio study on plane defects in zirconium-hydrogen solid solution and zirconium hydride, Acta Mater. 58 (11) (2010) 3927–3938, doi:10.1016/j.actamat.2010.03.034.
[31] C. Varvenne, O. Mackain, L. Proville, E. Clouet, Hydrogen and vacancy clustering in zirconium, Acta Mater. 102 (2016) 56–69, doi:10.1016/j.actamat.2015.09.019.